ADVANCED MATERIALS
www.advmat.de

Stretchable Energy-Harvesting Tactile Electronic Skin Capable of Differentiating Multiple Mechanical Stimuli Modes

Steve Park, Hyunjin Kim, Michael Vosgueritchian, Sangmo Cheon, Hyeok Kim, Ja Hoon Koo, Taeho Roy Kim, Sanghyo Lee, Gregory Schwartz, Hyuk Chang, and Zhenan Bao**

Human skin is one of the most complex and fascinating organs. It possesses a network of highly sensitive tactile sensors that are able to convert mechanical stimuli into physiological signals, which are then interpreted by the brain. In recent years, the field of electronic skin (e-skin) has attracted great interest in the research community due to its exciting potential applications such as touch-sensor-based prosthetics,[1–3] robotics with human-like functionalities (humanoids),[1–3] and continuous health monitoring.[4,5]

To mimic the properties of human skin, e-skin needs to have a high and appropriate range of tactile sensitivity. Secondly, distinguishing a variety of mechanical stimuli such as normal pressure, lateral strain, and bending is critical, as it allows object manipulation, grasp control, and texture determination. Thirdly, stretchability is important in placing e-skin conformably on arbitrarily curved and moving surfaces such as joints, and for it to withstanding repeated and prolonged mechanical stresses of various kinds such as bending and twisting.

Many groups have contributed to the advancement of e-skin over the past decade,[4–20] reporting increasing sensitivities. However, these pressure sensors did not have lateral stretchability and were not able to sense lateral strain. We have previously reported a stretchable pressure sensor array with carbon nanotube electrodes.[21] However, this device exhibited a relatively low pressure sensitivity on the order of 10^{-4} kPa^{-1}, and did not have the ability to differentiate lateral strain versus pressure sensing. More recently, stretchable resistive pressure sensors[22] and strain sensors[23–28] were demonstrated; however, these devices either lacked strain-sensing[22] or pressure-sensing capability.[23–28] Hence, fabricating devices with high pressure and strain sensitivity, intrinsic stretchability, and with the capability of distinguishing between various forms of tactile information remains a challenge.

Another important requirement for e-skin devices is a stretchable power source, which would allow the power source to be fully embedded in the e-skin device. Moreover, supplying self-sustainable power is important as it can negate the need to periodically replace the power source. Along this line, incorporating stretchable energy harvesting devices capable of converting mechanical stimuli to electric energy would be very useful in e-skin devices as e-skin devices are constantly under mechanical stimuli of various kinds during its operation. Harvesting mechanical energy has previously been achieved via piezoelectric phenomenon using materials like ZnO nanowires,[29–33] PVDF,[34–37] and $BaTiO_3$ nanocomposites.[38] In recent years, several groups have demonstrated mechanical energy harvesting using piezoelectric[39] and triboelectric effect[40–44] with pressure sensing capability. However, these devices have not demonstrated stretchability or differentiation of tactile information.

In this article, we present the first stretchable energy harvesting e-skin (EHES) that is able to detect, differentiate, and harvest a variety of mechanical stimuli, enabled by the stretchability of our device and a unique device architecture. To differentiate between various tactile information such as normal pressure, strain, and bending, we have utilized the stretchability of our device to simultaneously measure the change in capacitance and film resistance due to lateral strain. Our EHES had a high pressure sensitivity (average and maximum of 0.7 kPa^{-1} and 1.5 kPa^{-1} in the pressure region <1 kPa) compared to the previously reported stretchable capacitive pressure sensors.[20,21,45] In addition, our device was capable of harvesting various mechanical stimuli mentioned above with voltage and current generation in the range of tens of volts and tenths to several μA cm^{-2}, respectively. These features render our EHES unique and useful for a variety of e-skin applications

S. Park,[+] T. R. Kim
Stanford University
Department of Materials Science and Engineering,
496 Lomita Mall, Stanford, CA 94305-4034 USA
H. Kim,[+] H. Kim, H. Chang
Samsung Electronics Co.
Samsung Advanced Institute of Technology
130 Electronic Materials Research Complex
Samsung-ro, Gyeonggi-do, 443-803 South Korea
E-mail: hyunjin1.kim@samsung.com
M. Vosgueritchian, J. H. Koo, G. Schwartz, Z. Bao
Stanford University
Department of Chemical Engineering
Shriram Center
443 Via Ortega, Room 307, Stanford, CA 94305-4125, USA
E-mail: zbao@stanford.edu
S. Cheon
Center for Artificial Low Dimensional Electronic Systems
of the Institute for Basic Science
77 Cheongnam-ro, Pohang, 790-784 South Korea.
S. Lee
Hanyang University
Department of Physics
222 Wangsimni-ro, Seongdong-gu, Seoul, 133-791 South Korea

[+]These authors contributed equally to this work.

DOI: 10.1002/adma.201402574

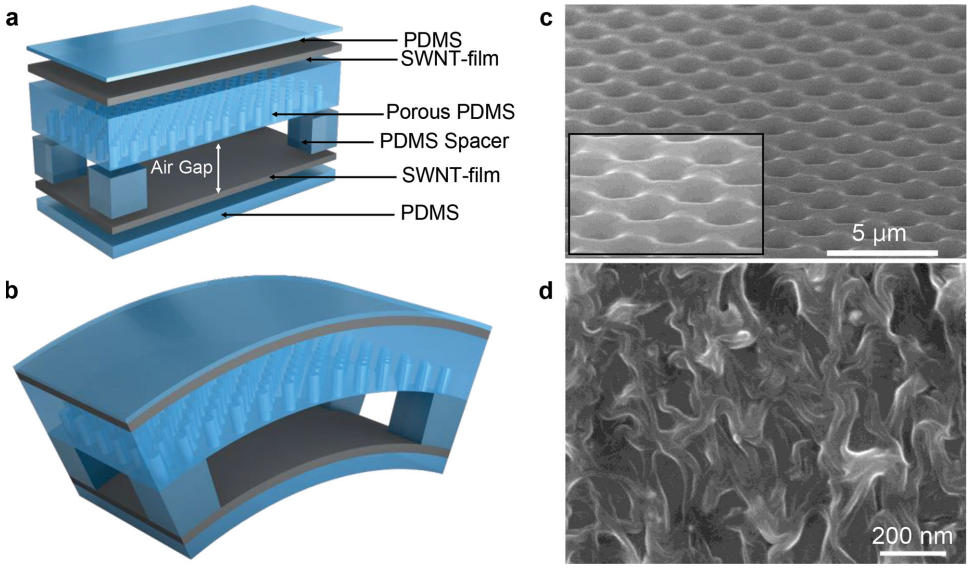

Figure 1. Device architecture. a) Schematic depiction of our EHES in a layer by layer format with description of each layer. b) Schematic depiction of our EHES with all of the layers combined. c) SEM image of the porous PDMS surface with an inset of high resolution SEM image. d) SEM image of buckled SWNTs on PDMS surface.

where conformable adherence to moving surfaces, multi-tactile sensing, and self-sustainable power is required, further advancing e-skin devices towards mimicking the properties and capabilities of human skin.

Figure 1a and 1b show schematic depictions of our EHES, which consists of (top to bottom) PDMS/SWNT-film/porous PDMS/PDMS spacers/SWNT-film/PDMS. Thin films of SWNTs were used as top and bottom electrodes while porous PDMS structure and air gap were used as dielectric layers. Negative charges on the porous PDMS surface were generated via UVO (ultraviolet ozone) with a surface charge density of ca. $-1.7\ \mu Cm^{-2}$ (measured using surface potentiometer, see Figure S3 in the Supporting Information). Even though temporal and thermal stability of charges on the PDMS surface is lower than that of the films with strong electret properties, the charges on the PDMS was effectively maintained during device operation as PDMS and the CNT film are repeatedly in contact with each other, causing triboelectric effect between PDMS and SWNT surface. Our EHES was uniquely designed to enable both highly sensitive pressure detection and electrical power generation. For a large pressure sensing dynamic range, air gap was implemented to sense pressure in the low pressure region (<1 kPa) while sensitivity in the higher pressure region (>1 kPa) was enabled using porous PDMS microstructuring. For energy harvesting, the air gap and charges on the PDMS surface was utilized to generate voltage and current.

Figure 1c and its inset show scanning electron microscopy (SEM) images of the porous PDMS surface, showing the regularly spaced 2 μm wide pores. The air gap was made by using PDMS spacers, which separated the porous PDMS structure and the bottom SWNT-film. PDMS was used as our main device component due to its intrinsic stretchability,[46,47] biocompatibility,[48,49] and its ability to conformably adhere to human skin.[50] To render the device stretchable, the electrode films needed to be stretchable. Silver nanowires[51–53] and carbon nanotubes [54–59] are some of the emerging materials for stretchable electrodes; for our work, we have elected to use SWNT-films for their relatively high stretchability, conductivity, and triboelectric properties with PDMS surface. Figure 1d is an SEM image of the SWNT-coated PDMS surface, showing the wavy conformation of the SWNTs. The wavy conformation was generated by straining and releasing the SWNT film by 50%, which buckles the SWNTs along the strain direction.[21] The sheet resistance of our device under no strain was 720 $\Omega\ \square^{-1}$, and increased by 10% at 30% strain. As described in our previous work,[21] the buckling of the SWNTs renders the film 'spring-like,' making the film highly stretchable. In this work, our devices were stretched up to 30%, which is typically what is required for e-skin applications.

Pressure sensing is conducted by detecting the change in the capacitance due to the change in the distance between the top and bottom electrodes. **Figure 2**a is a plot of change in capacitance ($\Delta C/C_o$) as a function of pressure, obtained using a device with unpatterned PDMS without an air gap (blue circles), porous PDMS without an air gap (red squares), unpatterned PDMS with a 0.7 mm air gap (green diamonds), and with porous PDMS with a 0.7 mm air gap (black triangles). Both the air gap and the porous PDMS were observed to increase the pressure sensitivity of our EHES. For the device with unpatterned PDMS surface without an air gap (blue circles), the slight increase in capacitance is due to the decrease in the distance between the top and bottom electrodes as the PDMS is compressed. Such a low sensitivity is due to the large pressure needed to compress a filled dielectric layer, which is also the cause of low sensitivity in previously reported pressure sensors with similar device architectures.[21,45] On the contrary, the device with porous PDMS without an air gap (red squares) yielded better pressure sensitivity due to the combined effect of less pressure required to deform the porous PDMS and air being driven out of the voids, changing the dielectric

Adv. Mater. **2014**,
DOI: 10.1002/adma.201402574

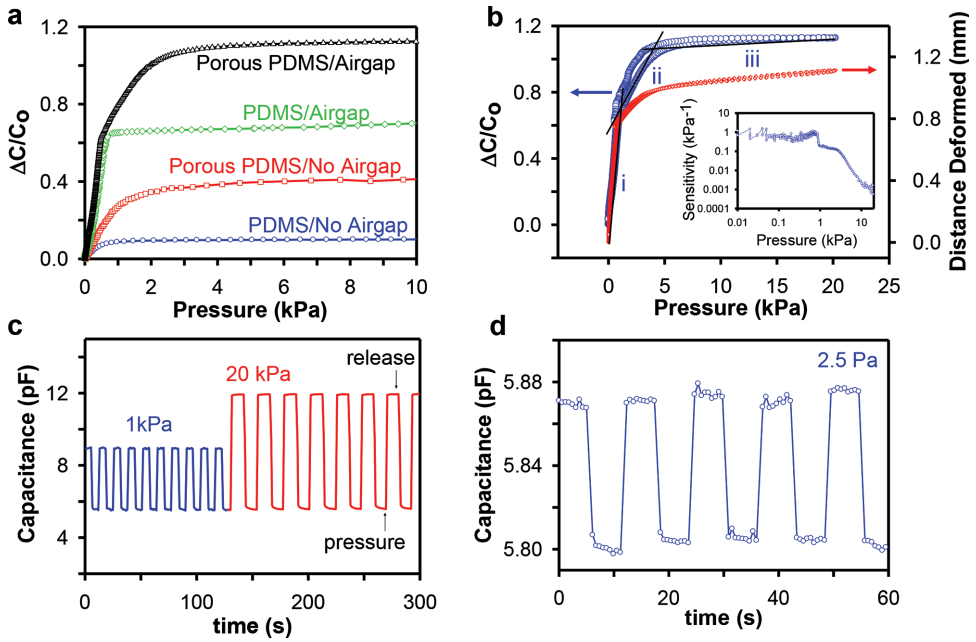

Figure 2. Pressure sensing. a) Plots of change in capacitance versus pressure using different devices. b) Plot of change in capacitance (blue circles) and distance deformed (red diamonds) as a function of pressure using a device with porous PDMS and an air gap. Inset is a plot of sensitivity ($S = \delta(\Delta C/C_o)/\delta p$) versus pressure in log scale. c) Capacitance versus time plot of the device represented in Figure 2b, under repeated normal pressure of 1 and 20 kPa. d) Capacitance versus time plot of the device represented in Figure 2b, under repeated normal pressure of 2.5 Pa.

constant as the PDMS is being compressed. When an air gap was implemented, sensitivity increased significantly in the low pressure region (green diamonds and black triangles). The air gap enables the distance between the top and bottom electrodes to change under relatively low pressures, resulting in a large rate of change in capacitance under small changes in pressure. The sharp change in the slope of the curves at approximately 1 kPa is due to the PDMS surface coming into contact with the bottom electrode, and is the point at which PDMS starts to deform. When an unpatterned PDMS layer was used with an air gap (green diamonds), sensitivity dropped significantly when the PDMS surface made contact with the bottom electrode, which as stated above, is due to the difficulty of deforming a filled dielectric layer. In addition, due to the strong adhesiveness of PDMS to the SWNT surface, a uniform PDMS thin-film layer could not be readily detached from the bottom SWNT electrode once it made contact, rendering it difficult to measure pressure repeatedly.

The highest overall pressure sensitivity was obtained when porous PDMS surface was used along with an air gap (black triangles), as the air gap enables high sensitivity in the low pressure region while the porous PDMS allows sensitive response in the higher pressure region. In addition, the porous surface of PDMS made it non-adhesive to the bottom SWNT electrode due to its reduced contact area, enabling repeated pressure sensing. As seen in Figure 2b, both the change in capacitance and distance deformed undergoes a sharp change in slope at around 1 kPa, an indication of PDMS surface coming in contact with the bottom electrode. In region i of Figure 2b (pressure <1 kPa), the average sensitivity ($S = \delta(\Delta C/C_o)/\delta p$) was 0.7 kPa^{-1} with a maximum value at 1.5 kPa^{-1}. In region ii, where the porous PDMS is being deformed (pressure 1–5 kPa), the average sensitivity was 0.14 kPa^{-1}. In region iii (pressure >5 kPa), the sensitivity further reduced to 0.005 kPa^{-1} as PDMS is highly compressed, requiring higher pressure to further deform the PDMS.

The observed minor hysteresis in the capacitance versus pressure plot in Figure 2b is a result of finite relaxation time for the PDMS to revert back to the original state after mechanical stress is released, yielding slightly higher capacitance in the backward sweep than in the forward sweep. Upon the release of 1 kPa and 20 kPa of pressure, our devices returned to 97% of its original capacitance within ca. 1 s (Figure 2c). Figure 2d is a plot of capacitance versus time under an extremely low pressure of 2.5 Pa, showing a change in signal of 1.2%. The detection of such a low range of pressure is comparable to some of the best values currently reported.[11,14,19,20,40,41]

Detecting and distinguishing of various mechanical stimuli is an important feature of electronic skin, which remains a significant challenge. We have utilized the stretchability of our EHES to simultaneously measure the change in capacitance and the change in resistance of the top and bottom electrodes. As mentioned previously, the increase in capacitance is due to the decrease in the distance between the top and bottom electrodes; whereas, the increase in the resistance of the SWNT films under lateral strain is due to the increase in length of the film. Under normal pressure, we have observed a large increase in capacitance by 80%, while negligible change in the resistances of the top and bottom electrodes were observed due to the lack of lateral straining of the SWNT films (**Figure 3**a). Under bending, a non-linear change in capacitance as a function of bending angle is observed (Figure 3b and 3c) due to the varying rate of change in the distance between the two electrodes at different bending angles. The resistance of both the

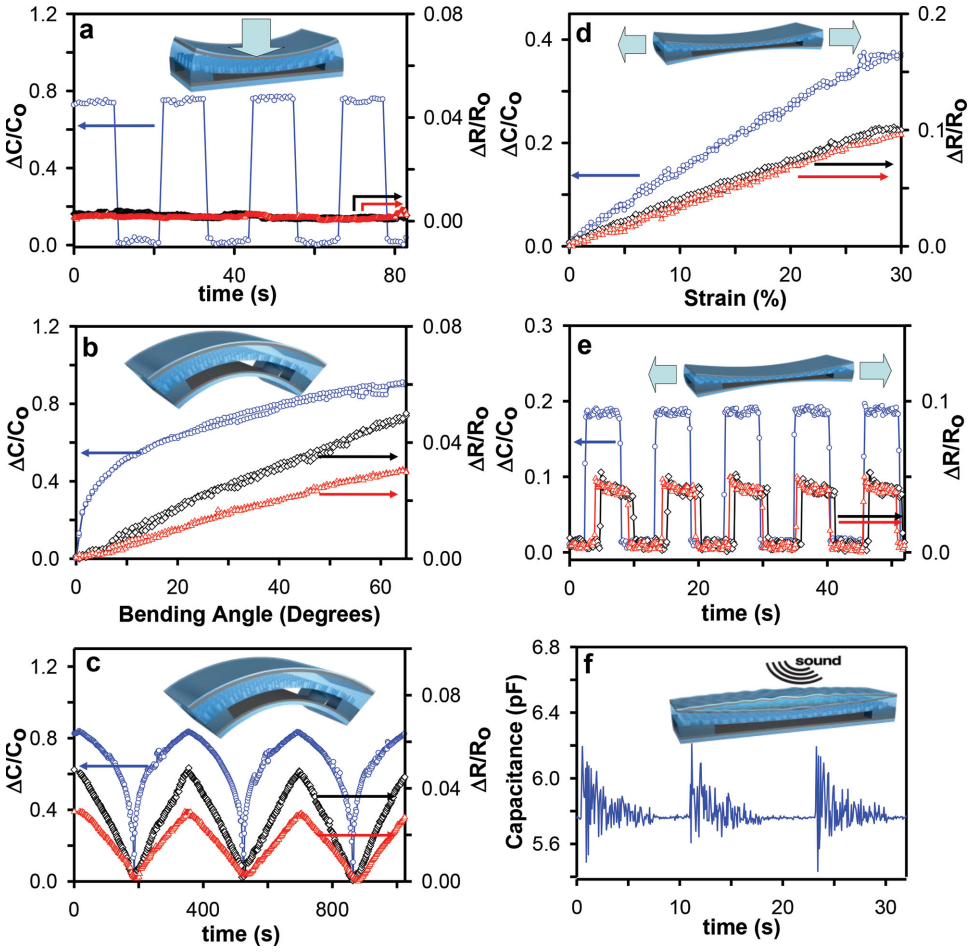

Figure 3. Detection of various mechanical stimuli. a) Capacitance and film resistances as a function of time under repeated normal pressure of 2 kPa. b) Capacitance and film resistances as a function of bending angle from 0 to 65°. c) Capacitance and film resistances as a function of time at incrementally increasing and decreasing bending angle from 0 to 65°. d) Capacitance and film resistances as a function of percent strained laterally e) and as a function of time at repeated strain of 15%. f) Capacitance as a function of time under sound vibration due to hitting a guitar string. a–e) Change in capacitance, change in top electrode resistance, and change in bottom electrode resistance are represented as blue circles, black diamonds, and red triangles, respectively.

top and bottom electrodes changes under bending due to lateral straining of the SWNT films. Lateral strain (ε) due to bending is related to the radius of curvature (R) by $\varepsilon = \gamma/R$, where γ is the position of the film with respect to the neutral axis. Hence, we expected the rate of change in resistance of the top electrode to be greater than that of the bottom electrode (since the top electrode is further away from the neutral axis), which is indeed what was observed experimentally. When the e-skin device is laterally stretched (Figure 3d and 3e), the distance between the two electrodes decreases due to poisson effect, resulting in an increase in capacitance.[21,52] The capacitive gauge factor ($\Delta C\ C_o^{-1}\ \varepsilon_{strain}^{-1}$) was calculated to be 1.3. The linearly increasing capacitance and resistances of the films as a function of strain was consistent with previously reported work.[21,52] Since the two electrodes are strained to the same amount under lateral strain, we have expectedly observed similar change in resistance of the top and bottom film. Our EHES was also used to detect sound-driven vibration. By placing our EHES on a speaker (which was connected to a guitar) and plucking a guitar string (sound intensity of ca. 80 dB), we have observed fluctuations in the capacitance of our EHES (no change in film resistance was observed as expected), where the magnitude of this fluctuation represented sound amplitude. As evident in Figure 3f, when a guitar string was plucked, the magnitude of fluctuation in the capacitance increased, and decreased gradually over approximately 6 s due to gradual sound dampening. The frequency of sound could not be detected due to the slow response time of our measurement apparatus. Further analysis is needed to fully verify the legitimacy of our device in being used as a microphone, and is the subject of our future work. These examples of detecting and distinguishing a variety of tactile information by observing the different behaviors in the change in capacitance and in the change in the film resistances render our EHES potentially useful in emulating human skin for a variety of touch sensor based applications.

Our capacitive sensor design also enables power generation through surface charges on the PDMS surface. The PDMS surface was initially negatively charged during UVO treatment and the surface charges were additionally generated and maintained through contact with the bottom SWNT electrode via

Adv. Mater. **2014**,
DOI: 10.1002/adma.201402574

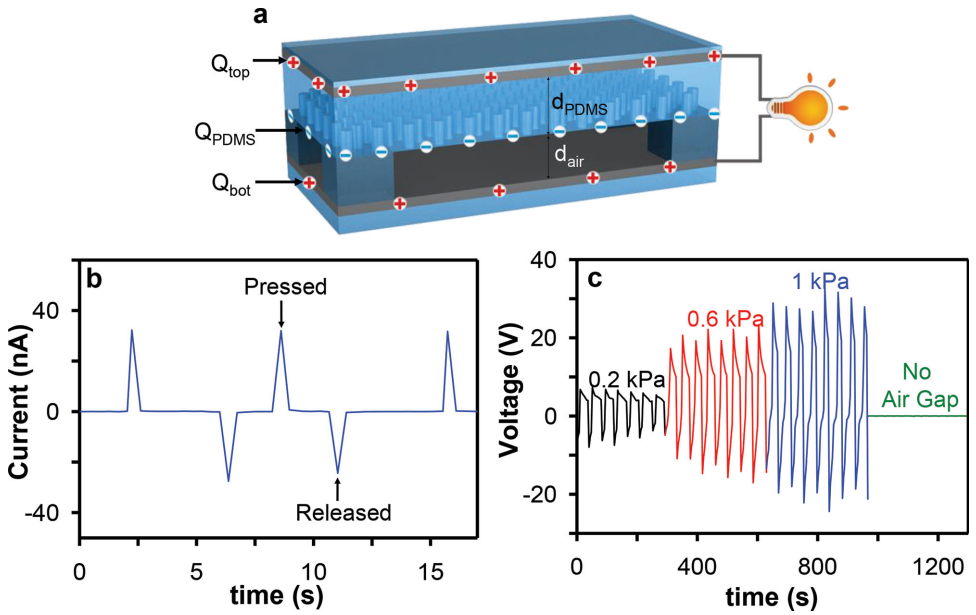

Figure 4. Energy-harvesting mechanism and characterization. a) Schematic depiction of our EHES for energy harvesting. b) Current generation as a function of time using 1 kPa of normal pressure and device area of 1 cm^2. c) Voltage generation under open-circuit conditions (resistance load of 10^{13} Ω) demonstrating linearly increasing voltage as a function of normal pressure. In addition, voltage generation of a device without an air gap is measured, showing significantly lower voltage generation than the device with an air gap.

triboelectric effect.[40,41,43,60–71] To balance the negative charges on the porous PDMS surface (Q_{PDMS}), positive charges accumulate on the top (Q_{top}) and bottom (Q_{bot}) electrodes so that:

$$|Q_{PDMS}| = |Q_{top} + Q_{bot}| \quad (1)$$

When pressure is applied and released, the distance between the electrodes changes. This causes charges to move back and forth between the top and bottom electrodes, resulting in current flow in the external circuit (see Supporting Information, section I, part I for more detailed explanation). As shown in **Figure 4**b, current is generated in opposite directions when pressure is applied and released, which is consistent with the mechanism proposed.

The total change in voltage (ΔV) can be expressed as:

$$\Delta V = \frac{Q_{bot}\Delta d_{air}}{\varepsilon_{air} A} \quad (2)$$

where Δd_{air} is the change in the air gap due to applied pressure, ε_{air} is the dielectric constant of air, and A is the area of the device (please refer to the Supporting Information, Section I, Part II for detailed derivation and further explanation). As seen in Figure 4c, the change in voltage (ΔV) linearly depended on the applied pressure, (yielding ΔV equal to 13, 32, and 48 V, respectively), which was consistent with the trend predicted by Equation 2 (in the low pressure region <1 kPa, pressure was linearly proportional to Δd_{air}). Also, worthy of noting here is that without an air gap, negligible voltage (and current) was generated, as depicted in Figure 4c. This further highlights the importance of an air gap in energy harvesting.

As discussed earlier, since power is generated through the change in the air gap, any movement that causes variation in the air gap can induce power generation. We have hence exploited the uniqueness of our EHES (stretchability and high sensitivity) to generate power from a wide-variety of mechanical stimuli. **Figure 5**a and Figure S4a in the Supporting Information show voltage and current generated as a function of time, respectively, by repeatedly pressing down onto our EHES using a finger with an approximate pressure of 2 kPa. Under such repeated normal pressure, a voltage and current range of 25 V and 8 μA cm^{-2} were generated, respectively. The power conversion efficiency was estimated to be ca. 8%. Recently, theoretically calculated power conversion efficiency of nanowire-based piezoelectric nanogenerators[72] was reported to be 1.8% to 5.58%. Hence, the efficiency of our device is comparably higher than the theoretical efficiency of nanowire-based piezoelectric devices. We have tested the durability of our EHES under repeated pressure and release of 1 kPa over 1000 cycles. As depicted in Figure S5 in the Supporting Information, we have determined that the same range of voltage was generated consistently over 1000 cycles, verifying the high durability of our e-skin under repeated pressure.

Other practically encountered stresses in skin are bending, torsion, and lateral tension. To test energy harvesting due to bending, our EHES was placed on a finger and was bent and released repeatedly at an angle of 75 °, as depicted in Figure 5b inset. As shown in Figure 5b and Figure S4b in the Supporting Information, this bending motion generated voltage and current range of 3 V and 0.25 μA cm^{-2}, respectively. Our EHES was also placed under repeated torsion to ±180°, as depicted in Figure 5c inset. As seen in Figure 5c and Figure S4c in the Supporting Information, voltage and current range of 10 V and 0.5 μA cm^{-2} were generated, respectively. Figure 5d and Figure S4d in the Supporting Information show voltage and current generation when our EHES was laterally strained to 10% and 30%, respectively. At 10% strain, voltage and current on the order of 8 V and 0.7 μA cm^{-2} was generated, respectively.

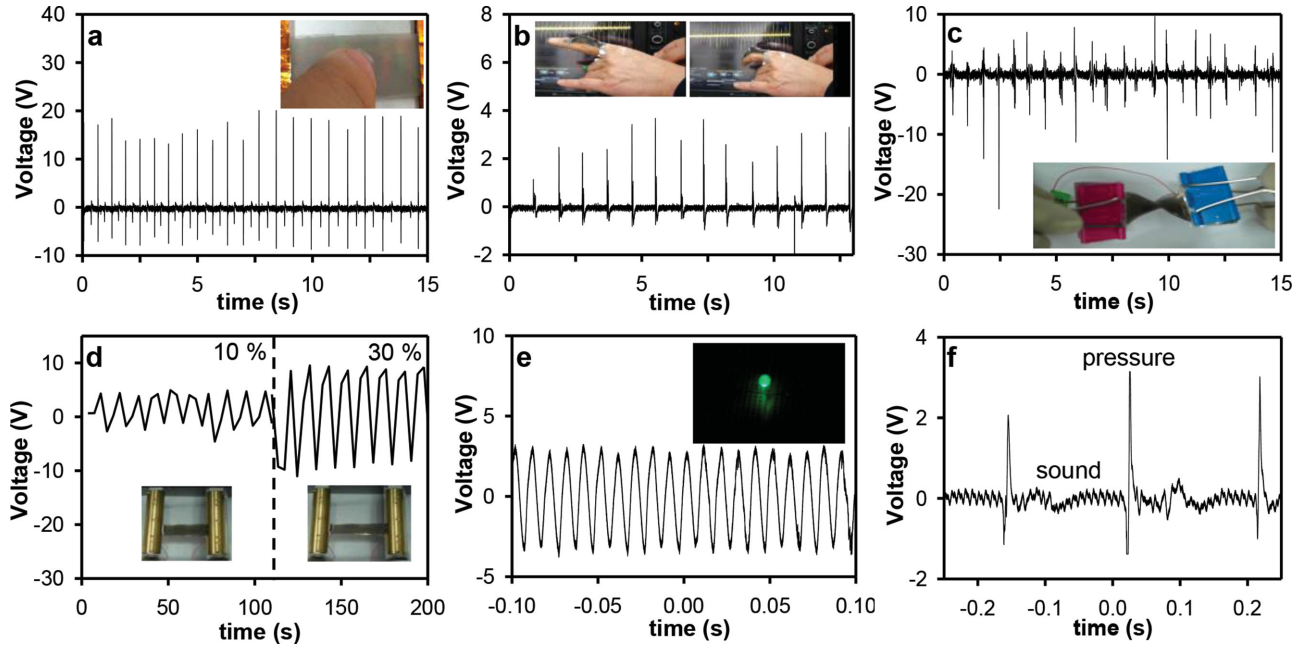

Figure 5. Energy harvesting from various mechanical stimuli. Voltage generation using: a) finger tapping with a pressure of ca. 2 kPa, b) bending to 75° after being attached on top of a finger, c) twisting to ±180°, d) lateral straining to 10% and 30%, and e) sound-driven vibration with sonic power and frequency of 100 dB and 100 Hz. The insets of (a–d) are images of the corresponding mechanical stress being applied. The inset of (e) is an image of a green LED being turned on using sound driven vibration. f) Voltage being generated with simultaneous sound-driven vibration and normal pressure applied using gentle finger tapping.

Sound-driven vibration was also demonstrated of being a viable source of energy. Our EHES was placed under an input sonic power and frequency of 100 dB and 100 Hz, respectively. As shown in Figure 5e and Figure S4e in the Supporting Information, the input sonic wave generated sinusoidal waves of voltage and current as a function of time, with a range of 6 V and 2 μA cm^{-2}, respectively. Using this AC voltage and current, we have used a rectifying circuit to convert the power to DC. The generated power was sufficient to turn on a green LED by charging up a 100 μF capacitor for 2 min (Figure 5e inset). Figure 5f and Figure S4f in the Supporting Information show the voltage and current as a function of time, respectively, under both a sound-driven vibration and normal pressure, demonstrating that power can be generated from different mechanical stresses simultaneously. Such versatility in harvesting a variety of mechanical energy sources is an important feature to efficiently harvest all of the mechanical stimuli that the e-skin device may be exposed to during its operation.

Position sensing is an important function in e-skin devices. To demonstrate the position sensing capacity of our e-skin, we have created a 5 × 5 pixel array with pixel area of 1 cm × 1 cm separated by 3 mm (**Figure 6**a and 6b). Figure 6c is a plot of the change in capacitance versus time, showing the response to 0.5 kPa of pressure at the pixel being pressed (black circles), and at one (red squares) and two (blue diamonds) pixels away. Evidently, the change in capacitance is the most dramatic at the pixel being pressed and decreases significantly going away from it. This feature is important for precise position sensing. The voltage generation was also observed to decrease moving away from the pixel being pressed with similar trends, as depicted in Figure 6d. Figure 6e is a 2D pressure map showing the change in capacitance and voltage generated at each pixel when the center pixel was pressed at 0.5 kPa. The resolution of our EHES can be improved using high resolution shadow masking or transfer printing,[73] which will ultimately enable the mimicking of position sensitivity of human skin. This is currently the subject of our future work.

Herein, we have demonstrated for the first time a stretchable energy-harvesting electronic skin (EHES) capable of sensing, differentiating, and harvesting a wide-variety of tactile information such as normal pressure, lateral strain, bending, and sound-driven vibration. Using PDMS microstructuring in combination with an air gap, we have enabled pressure sensing from several pascals to tens of kilopascals, with an average and maximum sensitivity of 0.7 kPa^{-1} and 1.5 kPa^{-1}, respectively, in the pressure region <1 kPa. Our pressure sensitivity was high in comparison to other stretchable capacitive pressure sensors: 0.23 kPa^{-1} (ref.[20]), 0.0004 (ref.[45]), 0.0002 kPa^{-1} (ref.[21]). We note that devices of higher sensitivities were fabricated using resistive sensing methodology,[4,14,22] or using transistor configuration.[5] However, these pressure sensors were not able to distinguish various mechanical stimuli. Our device, on the other hand, was capable of differentiating different tactile signals by measuring three different output signals (capacitance, resistance of the top and resistance of the bottom electrode). Here, our capacitive design was important since the top and the bottom electrodes needed to be electrically isolated so that the measured change in film resistance was only due to the lateral straining of each film, not due to the electrical conduction between the top and bottom electrodes. Several groups have previously measured signals coming from multiple mechanical stimuli.[16,21,24,45,74] However, these mechanical

Adv. Mater. **2014**,
DOI: 10.1002/adma.201402574

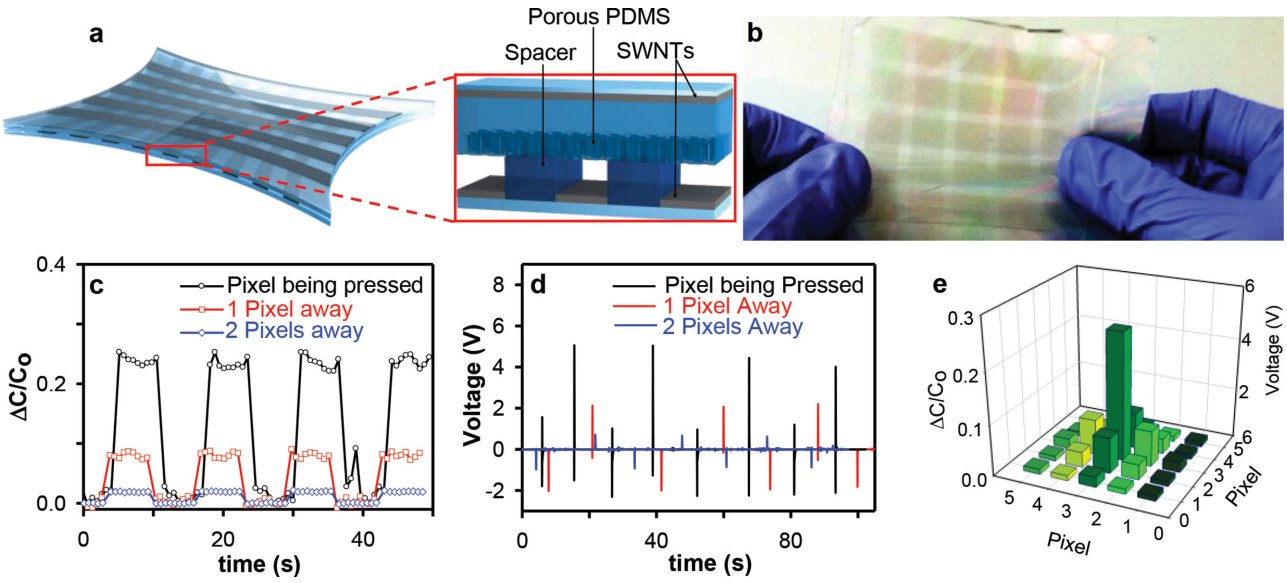

Figure 6. Position sensing using e-skin. a) Schematic representation of a position sensitive EHES with a cross sectional close-up image. b) Top view optical image of the position sensitive EHES. c) Change in capacitance at the pixel being pressed (black circles), and one (red squares) and two (blue diamonds) pixels away from the pixel being pressed. d) Change in voltage measured at the pixel being pressed (black), and one (red) and two (blue) pixels away from the pixel being pressed. e) 2D pressure map of the change in capacitance and voltage generation, with the center pixel being pressed at 0.5 kPa.

stimuli were measured with a single output signal (e.g., resistance or capacitance), rendering differentiation difficult. Other groups have demonstrated three axial force sensing;[75–78] however, these devices typically required complicated device architecture and were rarely made stretchable, rendering them difficult to measure and differentiate strain or bending. Our capacitive sensor design also enabled energy-harvesting functionality along with its sensing capability. We note that triboelectric energy-harvesting devices have previously used voltage or current as a signal to detect pressure.[40–44] However, rendering these devices stretchable and capable of differentiating different input signals remains to be a challenge. Voltage and current in the range of tens of volts and tenths to several μA cm^{-2} were generated using our EHES, respectively, yielding instantaneous power generation on the order of several to tens of μW cm^{-2}. Such an energy-harvesting functionality can potentially be utilized to not only operate e-skin device itself, but also power wearable health monitoring sensors (e.g., temperature sensor, ECG (electrocardiogram) sensor, blood pressure sensor).[79–81] Power generation can potentially be further improved through the enhancement of triboelectric effect (e.g., through the use of two surfaces with substantially different polarities)[60,82] or by inducing higher charge density on the dielectric surface using surface charging techniques.[83] In addition, implementation of stretchable capacitors[84] and battery[85] will be critical in enabling storage of generated power for continuous device operation. These are the subjects of our future work.

We envision that our energy-harvesting e-skin and the concepts introduced here can be utilized in the future to enable a fully self-sustainable skin-like devices with stretchability, multifunctional tactile sensing, and energy-harvesting capability.

Experimental Section

Preparation of PDMS Mold: A patterned silicon mold (with 2 μm wide and 100 μm tall pillars with a pitch of 4 μm) and a silicon wafer were treated with oxygen plasma for 1 min at 150 W. Subsequently, the silicon mold and the silicon wafer were placed in a vacuumed dessicator with a glass vial of 100 μL of (tridecafluoro-1,1,2,2-tetrahydrooctyl)-trichlorosilane for 4 h. This was to make the surface hydrophobic and ensure that the PDMS would not adhere to the surface of silicon. The PDMS used was SYLGARD 184 Silicone Elastomer Kit. To prepare the PDMS mixture, elastomer base was mixed with curing agent (60 g of elastomer base with 6 g of curing agent). The PDMS mixture was then poured onto the patterned silicon mold and the silicon wafer. The silicon mold and the silicon wafer were tilted the back and forth to ensure that PDMS was distributed evenly throughout all areas. The PDMS covered silicon mold and wafer were vacuumed in the dessicator for 2–3 h (or until the bubbles were no longer visible). It is important for the mold and the wafer to be leveled, as this will determine the PDMS thickness uniformity. Finally, the PDMS covered silicon mold and the silicon wafer were placed in an oven for 2 h at 70 °C to cure the PDMS. The thickness of the PDMS was between 0.5 to 0.7 mm.

Preparation of SWNT Solution: Arc-discharge SWNTs purchased from Hanwha Nanotech (Grade ASP-100F) were dispersed in NMP (N-methylpyrrolidinone) (1.5 mg in 15 mL) by sonicating the solution for 30 min in an ultrasonicator (Cole Parmer) at 30% amplitude. Subsequently, the solution was centrifuged at 10 000 rpm for 1 h, and the supernatant was extracted.

Spray Coating of SWNTs and Device Assembly: The PDMS-covered silicon mold and wafer were UVO-treated for 15 min with the PDMS side up, and then placed on a hot plate pre-heated to 190 °C. The SWNTs were uniformly spray coated on top of the PDMS surfaces (generally we used up ca. 5–6 mL of SWNT solution for a 4 in wafer area). To fabricate an array of electrodes (for position sensing devices), SWNTs were spray coated with a metal shadow mask (1 cm thick opening with 3 mm spacing) placed on top. Wire bonding was conducted using copper tape. The PDMS mixture with the aforementioned mixing ratio was spin-cast on the SWNT-film/PDMS/silicon mold structure at 8000 rpm for 10 min. The PDMS on the silicon mold was carefully peeled off, and was briefly treated with UVO for 20 s with the porous PDMS side up.

Finally, the PDMS on the silicon mold and on the wafer were stacked one on top of the other, with spacers sandwiched in between. The spacers were composed of PDMS, with diameter and thickness of 3 mm and 0.7–1 mm, respectively. For the pixilated devices, we oriented the parallel strips of the top and bottom electrodes perpendicular to each other to create a 5 by 5 pixel array with pixel area of 1 cm × 1 cm separated by 3 mm. PDMS spacers were placed at the corners of every pixel.

Device Characterization: Current and voltage measurements were conducted either using Keithley 4200-SCS (current measured with a short circuit, and voltage measured with an open circuit with current set to zero using an internal resistance of 10^{13} Ω) or using a close loop oscilloscope with internal resistance of 10^6 Ω. Capacitance and resistance measurements were conducted using Agilent E4980A, Precision LCR Meter. Pressure was measured using Mark-10 Model BG05 Series BG.

Supporting Information

Supporting Information is available from the Wiley Online Library or from the author.

Acknowledgments

This research was partially supported by MSIP (Ministry of Science), ICT (future planning), and Korea under the IT Consilience Creativity Program (NIPA-2014-H0201–14–1001) supervised by the NIPA (National IT Industry Promotion Agency). The authors thank Alex Leslie Chortos and Dr. Sungmin Kim for helpful discussions, and Dr. Myounghoon Jung for helping with LED lighting.

Received: June 11, 2014
Revised: August 2, 2014
Published online:

[1] V. Maheshwari, R. Saraf, *Angew. Chem Int. Ed.* **2008**, *47*, 7808.
[2] R. S. Dahiya, G. Metta, M. Valle, G. Sandini, *IEEE Trans. Robotics* **2010**, *26*, 1.
[3] C. Pang, C. Lee, K.-Y. Suh, *J. Appl. Polym. Sci.* **2013**, *130*, 1429.
[4] S. Gong, W. Schwalb, Y. Wang, Y. Chen, Y. Tang, J. Si, B. Schirinzadeh, W. Cheng, *Nat. Commun.* **2013**, *5*, 3132.
[5] G. Schwartz, B. C. K. Tee, J. Mei, A. L. Appleton, D. H. Kim, H. Wang, Z. Bao, *Nat. Commun.* **2013**, *4*, 1859.
[6] K. Takei, T. Takahashi, J. C. Ho, H. Ko, A. G. Gillies, P. W. Leu, R. S. Fearing, A. Javey, *Nat. Mater.* **2010**, *9*, 821.
[7] T. Someya, T. Sekitani, S. Iba, Y. Kato, H. Kawaguchi, T. Sakurai, *Proc. Natl. Acad. Sci. USA* **2004**, *101*, 9966.
[8] T. Someya, Y. Kato, T. Sekitani, S. Iba, Y. Noguchi, Y. Murase, H. Kawaguchi, T. Sakurai, *Proc. Natl. Acad. Sci. USA* **2005**, *102*, 12321.
[9] T. Takahashi, K. Takei, A. G. Gillies, R. S. Fearing, A. Javey, *Nano Lett.* **2011**, *11*, 5408.
[10] C. Wang, D. Hwang, Z. Yu, K. Takei, J. Park, T. Chen, B. Ma, A. Javey, *Nat. Mater.* **2013**, *12*, 899.
[11] S. C. B. Mannsfeld, B. C. K. Tee, R. M. Stoltenberg, C. Chen, S. Barman, B. V. O. Muir, A. N. Sokolov, C. Reese, Z. N. Bao, *Nat. Mater.* **2010**, *9*, 859.
[12] L. Hyung-Kew, C. Sun-Il, E. Yoon, *J. Microelectromech. Syst.* **2006**, *15*, 1681.
[13] M. Y. Cheng, X. H. Huang, C. W. Ma, Y. J. Yang, *J. Micromech. Microeng.* **2009**, *19*, 115001.
[14] L. Pan, A. Chortos, G. Yu, Y. Wang, S. Isaacson, R. Allen, Y. Shi, R. Dauskardt, Z. Bao, *Nat. Commun.* **2014**, *5*, 3002
[15] Q. Gao, H. Meguro, S. Okamoto, M. Kimura, *Langmuir* **2012**, *28*, 17593.
[16] C. Pang, G.-Y. Lee, T.-i. Kim, S. M. Kim, H. N. Kim, S.-H. Ahn, K.-Y. Suh, *Nat. Mater.* **2012**, *11*, 795.
[17] V. Maheshwari, R. F. Saraf, *Science* **2006**, *312*, 1501.
[18] M. Segev-Bar, A. Landman, M. Nir-Shapira, G. Shuster, H. Haick, *ACS Appl. Mater. Interfaces* **2013**, *5*, 5531.
[19] H.-B. Yao, J. Ge, C.-F. Wang, X. Wang, W. Hu, Z.-J. Zheng, Y. Ni, S.-H. Yu, *Adv. Mater.* **2013**, *25*, 6692.
[20] L. Xinchuan, Z. Yihao, M. W. Nomani, W. Xuejun, H. Tain-Yen, G. Koley, *J. Micromech. Microeng.* **2013**, *23*, 025022.
[21] D. J. Lipomi, M. Vosgueritchian, B. C. K. Tee, S. L. Hellstrom, J. A. Lee, C. H. Fox, Z. Bao, *Nat. Nanotechnol.* **2011**, *6*, 788.
[22] C.-L. Choong, M.-B. Shim, B.-S. Lee, S. Jeon, D.-S. Ko, T.-H. Kang, J. Bae, S. H. Lee, K.-E. Byun, J. Im, Y. J. Jeong, C. E. Park, J.-J. Park, U. I. Chung, *Adv. Mater.* **2014**, *26*, 3451.
[23] L. Cai, L. Song, P. Luan, Q. Zhang, N. Zhang, Q. Gao, D. Zhao, X. Zhang, M. Tu, F. Yang, W. Zhou, Q. Fan, J. Luo, W. Zhou, P. M. Ajayan, S. Xie, *Sci. Rep.* **2013**, *3*, 3048.
[24] T. Yamada, Y. Hayamizu, Y. Yamamoto, Y. Yomogida, A. Izadi-Najafabadi, D. N. Futaba, K. Hata, *Nat. Nanotechnol.* **2011**, *6*, 296.
[25] L. Lin, S. Liu, Q. Zhang, X. Li, M. Ji, H. Deng, Q. Fu, *ACS Appl. Mater. Interfaces* **2013**, *5*, 5815.
[26] D. J. Cohen, D. Mitra, K. Peterson, M. M. Maharbiz, *Nano Lett.* **2012**, *12*, 1821.
[27] R. Matsuzaki, T. Keating, A. Todoroki, N. Hiraoka, *Sens. Actuators, A* **2008**, *148*, 1.
[28] X. Xiao, L. Yuan, J. Zhong, T. Ding, Y. Liu, Z. Cai, Y. Rong, H. Han, J. Zhou, Z. L. Wang, *Adv. Mater.* **2011**, *23*, 5440.
[29] S. N. Cha, J. S. Seo, S. M. Kim, H. J. Kim, Y. J. Park, S. W. Kim, J. M. Kim, *Adv. Mater.* **2010**, *22*, 4726.
[30] X. Wang, J. Song, J. Liu, Z. L. Wang, *Science* **2007**, *316*, 102.
[31] Z. L. Wang, J. H. Song, *Science* **2006**, *312*, 242.
[32] H. Kim, S. M. Kim, H. Son, H. Kim, B. Park, J. Ku, J. I. Sohn, K. Im, J. E. Jang, J.-J. Park, O. Kim, S. Cha, Y. J. Park, *Energy Environ. Sci.* **2012**, *5*, 8932.
[33] S. Xu, Y. Qin, C. Xu, Y. Wei, R. Yang, Z. L. Wang, *Nat. Nanotechnol.* **2010**, *5*, 366.
[34] C. Chang, V. H. Tran, J. Wang, Y.-K. Fuh, L. Lin, *Nano Lett.* **2010**, *10*, 726.
[35] S. Cha, S. M. Kim, H. Kim, J. Ku, J. I. Sohn, Y. J. Park, B. G. Song, M. H. Jung, E. K. Lee, B. L. Choi, J. J. Park, Z. L. Wang, J. M. Kim, K. Kim, *Nano Lett.* **2011**, *11*, 5142.
[36] J. Chang, M. Dommer, C. Chang, L. Lin, *Nano Energy* **2012**, *1*, 356.
[37] J.-H. Lee, K. Y. Lee, M. K. Gupta, T. Y. Kim, D.-Y. Lee, J. Oh, C. Ryu, W. J. Yoo, C.-Y. Kang, S.-J. Yoon, J.-B. Yoo, S.-W. Kim, *Adv. Mater.* **2013**, *26*, 765.
[38] K.-I. Park, M. Lee, Y. Liu, S. Moon, G.-T. Hwang, G. Zhu, J. E. Kim, S. O. Kim, D. K. Kim, Z. L. Wang, K. J. Lee, *Adv. Mater.* **2012**, *24*, 2999.
[39] W. Wu, X. Wen, Z. L. Wang, *Science* **2013**, *340*, 952.
[40] F.-R. Fan, L. Lin, G. Zhu, W. Wu, R. Zhang, Z. L. Wang, *Nano Lett.* **2013**, *12*, 3109.
[41] L. Lin, Y. Xie, S. Wang, W. Wu, S. Niu, X. Wen, Z. L. Wang, *ACS Nano* **2013**, *7*, 8266.
[42] Z.-H. Lin, Y. Xie, Y. Yang, S. Wang, G. Zhu, Z. L. Wang, *ACS Nano* **2013**, *7*, 4554.
[43] Y. Yang, H. Zhang, Z.-H. Lin, Y. S. Zhou, Q. Jing, Y. Su, J. Yang, J. Chen, C. Hu, Z. L. Wang, *ACS Nano* **2013**, *7*, 9213.
[44] Y. Yang, H. Zhang, X. Zhong, F. Yi, R. Yu, Y. Zhang, Z. L. Wang, *ACS Appl. Mater. Interfaces* **2013**, *6*, 3680.
[45] D. P. J. Cotton, I. M. Graz, S. P. Lacour, *IEEE Sens. J.* **2009**, *9*, 2008.
[46] T. Sekitani, T. Someya, *Adv. Mater.* **2010**, *22*, 2228.

DOI: 10.1002/adma.201402574

[47] J. A. Rogers, T. Someya, Y. Huang, *Science* **2010**, *327*, 1603.
[48] Y. Mi, Y. Chan, D. Trau, P. Huang, E. Chen, *Polymer* **2006**, *47*, 5124.
[49] N. Q. Balaban, U. S. Schwarz, D. Riveline, P. Goichberg, G. Tzur, I. Sabanay, D. Mahalu, S. Safran, A. Bershadsky, L. Addadi, B. Geiger, *Nat. Cell Biol.* **2001**, *3*, 466.
[50] D.-H. Kim, N. Lu, R. Ma, Y.-S. Kim, R.-H. Kim, S. Wang, J. Wu, S. M. Won, H. Tao, A. Islam, K. J. Yu, T.-i. Kim, R. Chowdhury, M. Ying, L. Xu, M. Li, H.-J. Chung, H. Keum, M. McCormick, P. Liu, Y.-W. Zhang, F. G. Omenetto, Y. Huang, T. Coleman, J. A. Rogers, *Science* **2011**, *333*, 838.
[51] Z. Yu, Q. Zhang, L. Li, Q. Chen, X. Niu, J. Liu, Q. Pei, *Adv. Mater.* **2011**, *23*, 664.
[52] F. Xu, Y. Zhu, *Adv. Mater.* **2012**, *24*, 5117.
[53] M. Park, J. Im, M. Shin, Y. Min, J. Park, H. Cho, S. Park, M.-B. Shim, S. Jeon, D.-Y. Chung, J. Bae, J. Park, U. Jeong, K. Kim, *Nat. Nanotechnol.* **2012**, *7*, 803.
[54] T. Sekitani, H. Nakajima, H. Maeda, T. Fukushima, T. Aida, K. Hata, T. Someya, *Nat. Mater.* **2009**, *8*, 494.
[55] T. Sekitani, Y. Noguchi, K. Hata, T. Fukushima, T. Aida, T. Someya, *Science* **2008**, *321*, 1468.
[56] C. Feng, K. Liu, J.-S. Wu, L. Liu, J.-S. Cheng, Y. Zhang, Y. Sun, Q. Li, S. Fan, K. Jiang, *Adv. Funct. Mater.* **2010**, *20*, 885.
[57] L. Hu, W. Yuan, P. Brochu, G. Gruner, Q. Pei, *Appl. Phys. Lett.* **2009**, *94*, 161108.
[58] Z. Yu, X. Niu, Z. Liu, Q. Pei, *Adv. Mater.* **2011**, *23*, 3989.
[59] K.-Y. Chun, Y. Oh, J. Rho, J.-H. Ahn, Y.-J. Kim, H. R. Choi, S. Baik, *Nat. Nanotechnol.* **2010**, *5*, 853.
[60] S. Wang, L. Lin, Z. L. Wang, *Nano Lett.* **2012**, *12*, 6339.
[61] Y. Hu, J. Yang, Q. Jing, S. Niu, W. Wu, Z. L. Wang, *ACS Nano* **2013**, *7*, 10424.
[62] J. Yang, J. Chen, Y. Liu, W. Yang, Y. Su, Z. L. Wang, *ACS Nano* **2014**, *8*, 2649.
[63] G. Zhu, Z.-H. Lin, Q. Jing, P. Bai, C. Pan, Y. Yang, Y. Zhou, Z. L. Wang, *Nano Lett.* **2013**, *13*, 847.
[64] P. Bai, G. Zhu, Z.-H. Lin, Q. Jing, J. Chen, G. Zhang, J. Ma, Z. L. Wang, *ACS Nano* **2013**, *7*, 3713.
[65] J. Zhong, Q. Zhong, F. Fan, Y. Zhang, S. Wang, B. Hu, Z. L. Wang, J. Zhou, *Nano Energy* **2012**, *2*, 491.
[66] X.-S. Zhang, M.-D. Han, R.-X. Wang, F.-Y. Zhu, Z.-H. Li, W. Wang, H.-X. Zhang, *Nano Lett.* **2013**, *13*, 1168.
[67] S. Wang, Y. Xie, S. Niu, L. Lin, Z. L. Wang, *Adv. Mater.* **2014**, *26*, 2818.
[68] G. Cheng, Z.-H. Lin, Z. Du, Z. L. Wang, *Adv. Funct. Mater.* **2014**, *24*, 2892.
[69] L. Lin, S. Wang, Y. Xie, Q. Jing, S. Niu, Y. Hu, Z. L. Wang, *Nano Lett.* **2013**, *13*, 2916.
[70] Z. L. Wang, *ACS Nano* **2013**, *7*, 9533.
[71] S. Wang, L. Lin, Y. Xie, Q. Jing, S. Niu, Z. L. Wang, *Nano Lett.* **2013**, *13*, 2226.
[72] R. Hinchet, S. Lee, G. Ardila, L. Montès, M. Mouis, Z. L. Wang, *Adv. Funct. Mater.* **2013**, *24*, 971.
[73] F. N. Ishikawa, H.-k. Chang, K. Ryu, P.-c. Chen, A. Badmaev, L. Gomez De Arco, G. Shen, C. Zhou, *ACS Nano* **2008**, *3*, 73.
[74] L. Persano, C. Dagdeviren, Y. Su, Y. Zhang, S. Girardo, D. Pisignano, Y. Huang, J. A. Rogers, *Nat. Commun.* **2013**, *4*, 1633.
[75] R. Surapaneni, Q. Guo, Y. Xie, D. J. Young, C. H. Mastrangelo, *J. Micromech. Microeng.* **2013**, *23*, 075004.
[76] K. W. Liao, M. T. Hou, J. A. Yeh, *2013 Transducers & Eurosensors XXVII: 17th Int. Conf. on Solid-State Sensors, Actuators and Microsystems (TRANSDUCERS & EUROSENSORS XXVII)* **2013**, p. 1000.
[77] J. A. Dobrzynska, M. A. M. Gijs, *J. Micromech. Microeng.* **2013**, *23*, 11.
[78] H. K. Lee, J. Chung, S. I. Chang, E. Yoon, *J. Micromech. Microeng.* **2011**, *21*, 035101.
[79] C. J. Deepu, X. Y. Xu, X. D. Zou, L. B. Yao, Y. Lian, *Proc. Fifth IEEE Int. Workshop on Electronic Design, Test and Application (DELTA 2010)*, **2010**, p. 225.
[80] A. Pantelopoulos, N. G. Bourbakis, *IEEE Trans. Syst. Man Cybernetics, Part C* **2010**, *40*, 1.
[81] Z. Da Ren, C. J. Deepu, X. Xiao Yuan, L. Yong, *2011 IEEE Biomedical Circuits and Systems Conf. (BioCAS 2011)* **2011**, p. 205.
[82] G. Zhu, C. Pan, W. Guo, C.-Y. Chen, Y. Zhou, R. Yu, Z. L. Wang, *Nano Lett.* **2012**, *12*, 4960.
[83] R. Que, Q. Shao, Q. Li, M. Shao, S. Cai, S. Wang, S.-T. Lee, *Angew. Chem Int. Ed.* **2012**, *51*, 5418.
[84] T. Chen, H. Peng, M. Durstock, L. Dai, *Sci. Rep.* **2014**, *4*, 3612.
[85] S. Xu, Y. Zhang, J. Cho, J. Lee, X. Huang, L. Jia, J. A. Fan, Y. Su, J. Su, H. Zhang, H. Cheng, B. Lu, C. Yu, C. Chuang, T.-i. Kim, T. Song, K. Shigeta, S. Kang, C. Dagdeviren, I. Petrov, P. V. Braun, Y. Huang, U. Paik, J. A. Rogers, *Nat. Commun.* **2012**, *4*, 1543.